

Ghost Waves in Anisotropic Materials: negative refractive index and evanescent field enhancement in lossless media.

Evgenii Narimanov

School of Electrical and Computer Engineering, and Birck Nanotechnology Center, Purdue University, West Lafayette IN 47907

(Dated: April 24, 2017)

We show that transparent dielectrics with strong optical anisotropy support a new class of electromagnetic waves that combine the properties of propagating and evanescent fields. These “ghost waves” are created in tangent bifurcations that “annihilate” pairs of positive- and negative-index modes, and represent the optical analogue of the “ghost orbits” in the quantum theory of non-integrable dynamical systems.[1] Similarly to the regular evanescent fields, ghost waves support high transverse wavenumbers, but in addition to the exponential decay show oscillatory behavior in the direction of propagation. Ghost waves can be resonantly coupled to the incident evanescent waves, which then grow exponentially through the anisotropic media – as in the case of negative index materials.[2, 3] As ghost waves are supported by transparent dielectric media, they are free from the “curse” of material loss that is inherent to conventional negative index composites.

The recent development of negative index metamaterials, where the subwavelength structure of the composite unit cell allows simultaneously negative electric and magnetic response, [2] gave rise to the experimental demonstration of such unusual phenomena as negative refraction and backwards wave propagation [4], electromagnetic cloaking [5] and subwavelength focusing. [6] Particularly striking is the behavior of the evanescent waves which instead of the expected decay may show exponential growth through the negative index medium,[3] which offers the potential of to revolutionize the near-field optics.[7] However, this effect is only present when the metamaterial unit cell size is much smaller than the wavelength in the medium. [8] As a result, while there are many different realizations of the negative index media – from photonic crystals [9] to coupled Mie resonators [10] to plasmonic composites [11], it is only the latter class that supports this exponential enhancement of evanescent field.

However, the material loss inherent to plasmonic media due to the inevitable free-carrier absorption[12] severely limits the evanescent field enhancement [13] Despite multiple attempts to remove this stumbling block with new materials [14] or incorporating material gain in the composite design [15], the (nearly) “lossless metal” [16] that would allow the evanescent field control and amplification promised by metamaterial research for nearly two decades since the seminal work of J. Pendry, [3] remains an elusive goal.[14]

In this Letter, we present an alternative to the plasmonic approach. We demonstrate that strongly anisotropic dielectrics support “ghost waves” that differ from the “regular” propagating and evanescent fields. These ghost waves represent the optical analogue of the ghost orbits in the semiclassical theory of non-integrable systems. Similarly to the surface plasmons in negative index media, these ghost waves can resonantly couple to the incident evanescent field, resulting in its exponential “amplification” across the anisotropic media. However, all the primary component of the dielectric permittivity tensor for such the strongly anisotropic media that

supports the ghost waves, can be positive. As a result, the effect can be observed in a transparent and (nearly) lossless dielectric.

Due to the complexity of the fully three-dimensional nano-fabrication required for the metamaterials with simultaneously negative values of the dielectric permittivity and magnetic permeability, much attention was given to the possible alternatives that do not rely on the magnetic response.[17–19] If the desired negative index performance can be limited to the propagation in a waveguide, a number of such solutions are possible – using hyperbolic metamaterials, [18] Clarricoats-Waldrone geometry [17], or a waveguide with the core formed by biaxial anisotropic dielectric [19] – see Fig. 1(a). Note that in each of these solutions, the negative index modes appear in pairs with their positive index counterparts, with each pair born together at the same point of the system phase space at some critical frequency ω_c .

In direct proximity of ω_c , the mode dispersion $\omega(k_z)$ can be treated as a bifurcation diagram with the the frequency taking the role of the control parameter. Known as the tangent bifurcation, it is subject to the general rules of nonlinear dynamics,[20] such as e.g. the creation of new states in integer number of pairs. In particular, the actual mode spectra below the tangent bifurcation threshold show the signatures of the so called “ghost orbits” formally defined as extensions of the system dynamics to a higher-dimensional phase space (e.g. extended to complex time and/or spatial coordinates).[1] We therefore conclude that the negative index systems in a waveguide geometry that do not rely on magnetic response, [17–19] actually support optical equivalents of these “ghosts”. Furthermore, such optical ghost waves are essentially different from both positive- and negative-index modes.

While a waveguide with the core formed by a hyperbolic metamaterial, [18] will suffer high propagation loss due to the absorption in the hyperbolic medium, the approach based on biaxial dielectric media [19] is not so limited. Even with the metallic cladding (see Fig. 1(a)), the propagation loss will be relatively small, [24–

26] due to small field penetration into the metal. What is however more important, is that the mode pattern in the waveguide that is calculated for the “ideal metal” boundary conditions,[27] is identical to the standing wave formed by interfering plane waves incident on a planar dielectric layer, that does not at all involve any high-loss components – see Fig. 1(b). We will therefore use the waveguide geometry of Fig. 1(a) as the way to clarify the underlying dynamics and the physical origin of the ghost waves, followed by the generalization of our approach to its lossless counterpart of Fig. 1(b).

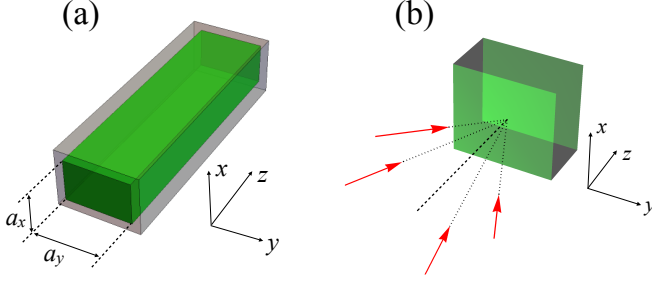


FIG. 1. The schematics of the metal-clad waveguide with the core formed by a biaxial anisotropic dielectric material (a), and the corresponding standing-standing wave pattern formed by the interference of several beams incident onto a slab of the biaxial anisotropic dielectric (b).

In the waveguide geometry of Fig. 1(a), the mode calculation is straightforward, and we obtain

$$k_z = \pm \frac{1}{\sqrt{2}} \left\{ (\epsilon_x + \epsilon_y) \left(\frac{\omega}{c} \right)^2 - \left(1 + \frac{\epsilon_x}{\epsilon_z} \right) q_x^2 - \left(1 + \frac{\epsilon_y}{\epsilon_z} \right) q_y^2 \pm \left[\left((\epsilon_x - \epsilon_y) \left(\frac{\omega}{c} \right)^2 + \left(1 - \frac{\epsilon_x}{\epsilon_z} \right) q_x^2 - \left(1 - \frac{\epsilon_y}{\epsilon_z} \right) q_y^2 \right)^2 + 4 \left(1 - \frac{\epsilon_x}{\epsilon_z} \right) \left(1 - \frac{\epsilon_y}{\epsilon_z} \right) q_x^2 q_y^2 \right]^{\frac{1}{2}} \right\}^{\frac{1}{2}}, \quad (1)$$

where different signs correspond to different “branches” of the dispersion diagram, and ϵ_x , ϵ_y and ϵ_z are the primary components of the dielectric permittivity tensor in the waveguide core. For the waveguide $q_x = m_x \pi / a_x$ and $q_y = m_y \pi / a_y$, where a_x and a_y represent the dimensions of the waveguide cross-section (see Fig. 1(a)), while in the 3D case of Fig. 1(b) q_x and q_y correspond to the magnitudes of the in-plane momentum components of the incident wave(s). If one of the integers m_x and m_y is equal to zero, the propagating fields are either TE- or TM-polarized, otherwise the mode has the “hybrid” structure [25] when all six components of the electromagnetic field are nonzero.

Choosing \hat{x} as the direction of the largest permittivity in the (x, y) plane (i.e. $\epsilon_x < \epsilon_y$), we find (see Fig. 2) that the system supports negative index modes (with the

group velocity $v_z = \partial\omega / \partial k_z < 0$) if and only if

$$\epsilon_x < \epsilon_z < \epsilon_y, \quad (2)$$

and

$$\arctan \left[\frac{\epsilon_x}{\epsilon_y} \sqrt{\frac{\epsilon_y - \epsilon_z}{\epsilon_z - \epsilon_x}} \right] < \theta < \arctan \left[\sqrt{\frac{\epsilon_y - \epsilon_z}{\epsilon_z - \epsilon_x}} \right], \quad (3)$$

where the angle

$$\theta \equiv \arctan [q_y / q_x] \quad (4)$$

in the waveguide geometry (Fig. 1(a)) is defined by the dimensions of the waveguide cross-section ($\theta = \arctan [m_y a_x / m_x a_y]$), while for the 3D case (see Fig. 1(b)) the angle θ corresponds to the propagation direction in the (x, y) plane. This is consistent with the results of Ref. [19], where the presence of negative index modes in biaxial anisotropic media waveguides was first pointed out.

Furthermore, when θ is equal to

$$\theta_D = \arctan \left[\sqrt{\frac{\epsilon_x}{\epsilon_y} \cdot \frac{\epsilon_y - \epsilon_z}{\epsilon_z - \epsilon_x}} \right], \quad (5)$$

we find that the system shows Dirac dispersion point at the frequency

$$\omega_D = c \sqrt{\frac{(\epsilon_y - \epsilon_x)}{\epsilon_y (\epsilon_z - \epsilon_x)}} \cdot q_x, \quad (6)$$

as seen in Fig. 2(b). Note that, as follows from Eqns. (5) and (6), the anisotropic waveguide system only shows the Dirac point when all three primary components of its dielectric permittivity tensor are different from each other.

For a given set of the integers m_x and m_y (or equivalently for a given magnitude of the in-plane momentum on the incident field (q_x, q_y) (see Fig. 1(a)), the biaxial anisotropic dielectric core supports propagating waves only above the critical frequency (see Fig. 2)

$$\omega_c = \frac{c}{\sqrt{\epsilon_y - \epsilon_x}} \left(q_x \sqrt{\frac{\epsilon_z}{\epsilon_x} - 1} + q_y \sqrt{\frac{\epsilon_z}{\epsilon_x} - 1} \right), \quad (7)$$

when two simultaneous tangent bifurcations, one at $k_z = k_c$ and the other at $k_z = -k_c$, where

$$k_c = \frac{1}{\sqrt{\epsilon_z (\epsilon_y - \epsilon_x)}} \left\{ \epsilon_x (\epsilon_z - \epsilon_y) q_x^2 + \epsilon_y (\epsilon_x - \epsilon_z) q_y^2 + (\epsilon_x + \epsilon_y) \sqrt{(\epsilon_z - \epsilon_x) (\epsilon_y - \epsilon_z) q_x q_y} \right\}^{1/2}, \quad (8)$$

create two pairs of positive and negative-index modes. However, if – following the standard approach originally developed for the semiclassical dynamics of non-integrable systems,[1, 21–23] – one extends the system phase space to the complex domain, Eqn. (1) also yields two pairs of solutions below the critical frequency ω_c ,

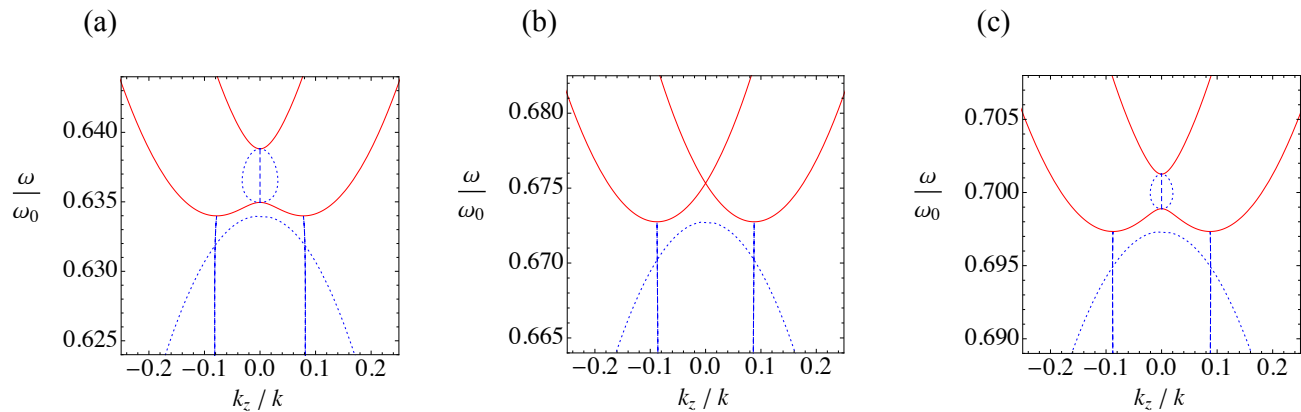


FIG. 2. The dispersion diagrams for the waves supported by sodium nitrite NaNO_2 , a biaxial anisotropic dielectric with the primary components of the dielectric permittivity tensor [19, 31] $\epsilon_x \simeq 1.806$, $\epsilon_y \simeq 2.726$ and $\epsilon_z \simeq 1.991$, with the frequency in units of ω_0 and the wavenumber k_z in units of $k \equiv \omega_0/c$, for $q_x = 0.5 k_0$, $q_y = 0.75 k_0$ (a), $q_x = 0.5 k_0$, $q_y = 0.81 k_0$ (b), and $q_x = 0.5 k_0$, $q_y = 0.85 k_0$ (c), where $k_0 \equiv \omega_0/c$ is the free space wavenumber at the frequency ω_0 . For the waveguide system in Fig. 1(a), $q_x = \pi m_x/a_x$ and $q_y = \pi m_y/a_y$, where m_x and m_y are positive integer numbers, while for the anisotropic dielectric slab geometry in Fig. 1(b) q_x and q_y correspond to the magnitudes of the (in-plane) x - and y - components of the incident field wavevector. Note the Dirac point in (b) at the frequency $\omega \approx 0.675 \omega_0$. Red lines represent the propagating modes, while blue curves correspond to the ghost waves, with dashed and dotted lines showing the real and the imaginary parts of the wavenumber k_z .

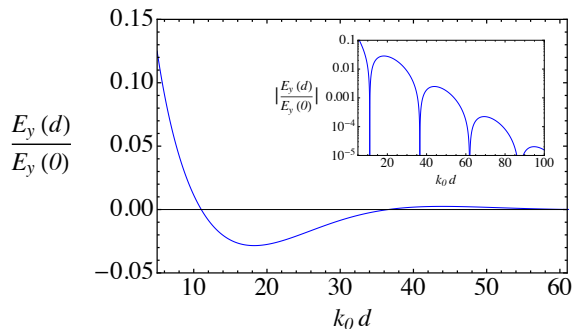


FIG. 3. The y -component of the electric field in the biaxial anisotropic dielectric slab as a function of the slab width d . The dielectric occupies the range $0 < z < d$ (see also the schematics in Fig. 4(a,b)), $q_x \simeq 0.79 k_0$ and $q_y \simeq 0.185 k_0$. The surrounding medium is air, and the anisotropic dielectric is sodium nitrite NaNO_2 . The inset shows the field in the logarithmic scale. Note the combination of the exponential decay and the oscillatory behavior, characteristic of the ghost waves.

with complex-conjugate wavenumbers that have simultaneously nonzero real and imaginary parts: $\pm k'_z \pm i k''_z$, as shown in Fig. 2 by blue lines. These new modes are the optical equivalents to the “ghost” solutions in non-linear dynamics.[1]

Qualitatively, the ghost fields combine the properties of the evanescent and propagating waves. Similarly to the evanescent modes, the intensity of the ghosts waves exponentially decays with distance. On the other hand, the ghost waves also oscillate – which allows to use con-

ventional interference to control their propagation. The latter behavior is illustrated in Fig. 3, corresponding to a biaxial dielectric of length d inserted into the originally air-field metal waveguide (see Fig. 4(a)) that is operating below the cut-off frequency ω_c , or to a biaxial dielectric slab of the width d (see Fig. 4(b)). As a function of the length d , the field in the dielectric shows both the exponential decay and the oscillations, consistent with the picture of the excitation of the ghost waves.

The most important feature of the ghost waves, however, is that they can be resonantly coupled to the incident evanescent wave. In this regime, within the biaxial dielectric supporting the ghost waves, the evanescent decay is replaced by the exponential increase of the field amplitude – as seen in Fig. 4. Aside from the oscillatory behavior of the ghost waves “under” the exponential envelope, this behavior is similar to that in the negative index superlens that also shows exponential “amplification” of the evanescent field. [3] However, as the ghost waves can be supported by a dielectric slab that does not include any lossy components such as metals (see Fig. 4(b)), the ghost waves are free from the constraint of the material absorption that severely limits the superlens performance.

The fundamental physical origin of the exponential “amplification” in biaxial media is also similar to that in the negative index superlens, – it’s the resonant coupling to surface states supported by the medium.[32] In the case of the negative index material - air interface, the surface state in question is the surface plasmon-polariton,[11, 32] while in the biaxial dielectric it’s the surface mode at the isotropic dielectric - anisotropic dielectric interface, shown in Fig. 5. This surface modes is

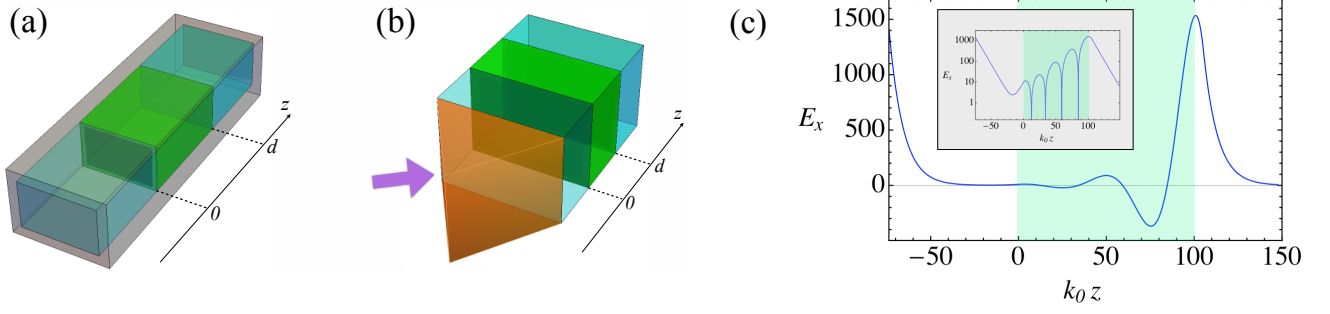


FIG. 4. Evanescent field enhancement at the ghost resonance, in the waveguide (a) and in slab geometry (b). Green region represents the biaxial anisotropic dielectric, blue is the surrounding dielectric medium, and orange is the high-index prism coupler. Panel (c) shows the x -component of the electric field, with the linear scale in the main plot and the logarithmic scale in the inset. The green-shaded areas in panel (c) and its inset indicate the range occupied by the anisotropic dielectric medium. In this example, the anisotropic dielectric is sodium nitrite NaNO_2 with the width $d \simeq 16.18 \lambda_0$, and the surrounding medium is sugar solution with the permittivity of $\epsilon_0 = 2.01$, $q_x \simeq 0.793 k_0$ and $q_y \simeq 1.182 k_0$. Note the dramatic enhancement of the incident evanescent field in the anisotropic material.

formed by the “regular” evanescent field in the isotropic side, and by the decaying ghost wave in the biaxial medium (note the oscillatory behavior for $z > 0$ in Fig. 5). In the limit $\epsilon_z \rightarrow \epsilon_x$ this mode reduces to the well-known Dyakonov surface wave that was originally introduced for the interface of an isroptic medium with a uniaxial dielectric.[28–30]

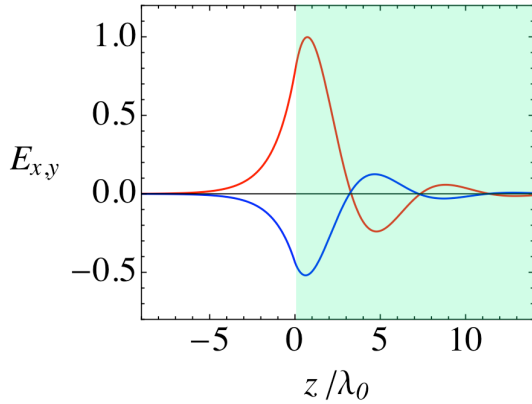


FIG. 5. The surface state profile at the interface of isotropic dielectric with biaxial anisotropic medium. The red and blue lines respectively correspond to the x - and y - components of the electric field. The biaxial dielectric is sodium nitrite NaNO_2 ($\epsilon_x \simeq 1.806$, $\epsilon_y \simeq 2.726$, $\epsilon_z \simeq 1.991$), the isotropic medium is sugar solution ($\epsilon = 2.01$), $q_x \simeq 0.793 k_0$ and $q_y \simeq 1.182 k_0$. Note the simple exponential decay in the isotropic material and oscillatory behavior in the biaxial medium.

At the interface of the biaxial medium and the isotropic dielectric with the permittivity ϵ_0 , the surface state dis-

persion $\omega_s(q_x, q_y)$ is defined by the equation

$$\begin{aligned} & \kappa_0 (\kappa_+ + \kappa_-) \left\{ \kappa_+ \kappa_- + \frac{\epsilon_x \epsilon_y}{\epsilon_0} \left(\frac{q_x^2}{\epsilon_y} + \frac{q_y^2}{\epsilon_x} - \left(\frac{\omega_s}{c} \right)^2 \right) \right\} \\ & + \kappa_+ \kappa_- \left\{ \left(1 + \frac{\epsilon_x}{\epsilon_0} \right) q_x^2 + \left(1 + \frac{\epsilon_y}{\epsilon_0} \right) q_y^2 \right. \\ & \left. - (\epsilon_x + \epsilon_y) \left(\frac{\omega_s}{c} \right)^2 \right\} \\ & + \left\{ \kappa_+^2 \kappa_-^2 + \frac{\epsilon_x \epsilon_y}{\epsilon_0} \kappa_0^2 \left(\frac{q_x^2}{\epsilon_y} + \frac{q_y^2}{\epsilon_x} - \left(\frac{\omega_s}{c} \right)^2 \right) \right\} = 0, \quad (9) \end{aligned}$$

where

$$\kappa_0 = \sqrt{q_x^2 + q_y^2 - \epsilon_0 \left(\frac{\omega_s}{c} \right)^2}, \quad (10)$$

and

$$\begin{aligned} \kappa_{\pm} = & \frac{1}{\sqrt{2}} \left\{ \left(1 + \frac{\epsilon_x}{\epsilon_z} \right) q_x^2 + \left(1 + \frac{\epsilon_y}{\epsilon_z} \right) q_y^2 \right. \\ & \left. - (\epsilon_x + \epsilon_y) \left(\frac{\omega_s}{c} \right)^2 \pm \left[\left((\epsilon_x - \epsilon_y) \left(\frac{\omega_s}{c} \right)^2 \right)^2 \right. \right. \\ & \left. \left. + \left(1 - \frac{\epsilon_x}{\epsilon_z} \right) q_x^2 - \left(1 - \frac{\epsilon_y}{\epsilon_z} \right) q_y^2 \right]^2 \right. \\ & \left. + 4 \left(1 - \frac{\epsilon_x}{\epsilon_z} \right) \left(1 - \frac{\epsilon_y}{\epsilon_z} \right) q_x^2 q_y^2 \right]^{1/2} \right\}^{1/2}. \quad (11) \end{aligned}$$

Note that Eqn. (9) has a solution only when $\epsilon_z < \epsilon_0 < \epsilon_y$.

As a function of frequency, the transmission coefficient for the incident evanescent field shows a very sharp resonance which becomes progressively more narrow with the increase of the width of the anisotropic layer d – see Fig. 6. Note that close to the center of this “ghost resonance” its profile shows the double-peak structure, corresponding to the symmetric and anti-symmetric combination of the surface states at the two interfaces. An increase

of the width of the anisotropic layer reduces the coupling between these two surface states, which reduces the splitting between the peaks – see Fig. 6.

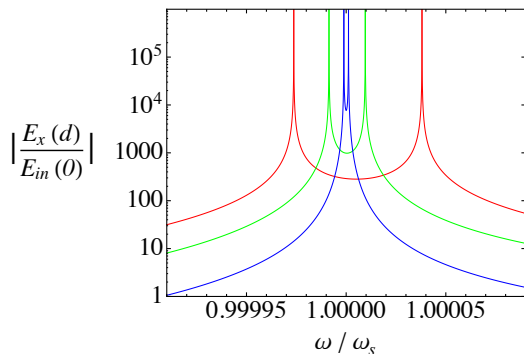


FIG. 6. The frequency spectrum of the “transmitted” field $E_x(d)$, normalized to the amplitude of the incident field E_{in} at $z = 0$ (see the schematics in Fig. 4(a),(b)), for the sodium nitrite biaxial crystal slab (green region in Fig. 4(a),(b)), surrounded by sugar solution with the permittivity $\epsilon = 2.01$ (shown in blue in Fig. 4(a),(b)), with $q_x \simeq 0.79 k_0$ and $q_y \simeq 1.18 k_0$. The width of the dielectric slab $d \simeq 7.96 \lambda_0$ (red curve), $d \simeq 11.94 \lambda_0$ (green curve) and $d \simeq 16.78 \lambda_0$ (blue curve). The frequency is normalized to the value corresponding to the surface state at a single sodium nitrite - sugar solution interface, given by Eqn. (9).

While for the idealized model of the system (lossless dielectric, perfect planar interfaces, no bulk defects leading to light scattering), the transmission coefficient at the ghost resonance can be arbitrary high, any disorder will limit the field enhancement. While these imperfection and their impact can be, at least in theory, reduced to an arbitrarily small level, these is also a fundamental limit to the performance of the proposed “ghost resonator,” imposed by the inherent non-locality of the electromagnetic response due to the final size of the material unit cell. For natural dielectric media, the corresponding correction to the permittivity scales [33] as $(k_0 a_0)^2$, where a_0 is on the order of the atomic/molecular size, leading to the fundamental limit on the evanescent field enhancement $\sim 1/(k_0 a_0)^2 \sim 10^5$.

In conclusion, we have demonstrated that biaxial anisotropic media supports ghost waves that combine the properties of the propagating and the evanescent fields. We have shown that resonant coupling of the ghost modes can be used to exponentially enhance and modulate the incident evanescent waves, thus opening a new way of the near field control and manipulation.

This work was partially supported by the National Science Foundation (grant 1629276-DMR), Army Research Office (grant W911NF-14-1-0639) and Gordon and Betty Moore Foundation.

-
- [1] M. Kuś, F. Haake, and D. Delande, “Prebifurcation periodic ghost orbits in semiclassical quantization,” *Phys. Rev. Lett.* **71**, 2167 (1993).
- [2] Veselago, V. G. , “The Electrodynamics of Substances with Simultaneously Negative Values of ϵ and μ ,” *Sov.Phys. – Usp.***10**, 509 - 518 (1968).
- [3] J. B. Pendry, “Negative Refraction Makes a Perfect Lens,” *Phys. Rev. Lett.* **85**, 3966 (2000).
- [4] R. A. Shelby, D. R. Smith, S. Schultz, “Experimental Verification of a Negative Index of Refraction,” *Science* **292**, 77 - 79 (2001).
- [5] Schurig, D.; et al.”Metamaterial Electromagnetic Cloak at Microwave Frequencies”. *Science* **314** (5801), 977 - 980 (2006).
- [6] A. Grbic and G.V. Eleftheriades, “Negative refraction, growing evanescent waves and sub-diffraction imaging in loaded-transmission-line metamaterials,” *IEEE Trans. on Microwave Theory and Techniques* **51** (12), 2297- 2305 (2003).
- [7] Z. Liu, N. Fang, T.-J. Yen, and X. Zhang, “Rapid growth of evanescent wave by a silver superlens,” *Appl. Phys. Lett.* **83** (25), 5184 - 5186 (2003).
- [8] R. Merlin, “Metamaterials and the LandauLifshitz permeability argument: Large permittivity begets high-frequency magnetism,” *Proc. Nat. Academy of Science* **106** (6), 1693 - 1698 (2008).
- [9] C. Luo, S. G. Johnson, and J. D. Joannopoulos, “All-angle negative refraction in a three-dimensionally periodic photonic crystal,” *App. Phys. Lett.* **81** (13), 2352 - 2354 (2002).
- [10] M. S. Wheeler, J. S. Aitchison, and M. Mojahedi, “Coated nonmagnetic spheres with a negative index of refraction at infrared frequencies,” *Phys. Rev. B* **73**, 045105 (2006).
- [11] W. Can and V. Shalaev, “Optical Metamaterials: Fundamentals and Applications,” Springer, New York (2010).
- [12] The situation is similar in polaritonic materials in mid-IR wavelength range, where the negative permittivity originated from resonant coupling to optical phonons, with the concomitant “resonant” loss. [11]
- [13] V. A. Podolskiy and E.i E. Narimanov, “Near-sighted superlens,” *Optics Letters* **30** (1), 75 - 77 (2005).
- [14] G.V. Naik, V.M. Shalaev, and A. Boltasseva, *Alternative Plasmonic Materials: Beyond Gold and Silver*, *Advanced Materials* **25** (24), 3264 - 3294 (2013).
- [15] S. Xiao *et al*, “Loss-free and active optical negative-index metamaterials,” *Nature* **466**, 735 - 738 (2010).
- [16] J. B. Khurgin, and G. Sun, “In search of the elusive lossless metal,” *Appl. Phys. Lett.* **96**, 181102 (2010).
- [17] A.S alandrino and D. N. Christodoulides, “Negative index Clarricoats-Waldron waveguides for terahertz and far infrared applications,” *Opt. Express* **18** (4), 3626 - 3631 (2010).
- [18] L. V. Alekseyev and E. Narimanov, “Slow light and 3D imaging with non-magnetic negative index systems,” *Optics Express* **14** (23), 11184 - 11193 (2006).
- [19] J. Nemirovsky, M. C. Rechtsman, and M. Segev, “Negative radiation pressure and negative effective refractive

- index via dielectric birefringence,” *Optics Express* **20** (8), 8907 - 8914 (2012).
- [20] F. Haake, “Quantum Signatures of Chaos,” Springer, New York (2010).
- [21] R. Scharf and B. Sundaram, “Traces of ghost orbits in the quantum standard map,” *Phys. Rev. E* **49**, R4767 (1994).
- [22] T. Bartschdag, J. Maindag and G. Wunnerddag, “Significance of ghost orbit bifurcations in semiclassical spectra,” *Journal of Physics A: Mathematical and General* **32** (16), 3013 - 3028 (1999).
- [23] B. Grmaud and D. Delande, “Ghost orbits in the diamagnetic hydrogen spectrum using harmonic inversion,” *Phys. Rev. A* **61**, 032504 (2000).
- [24] Even at optical frequencies, one finds the effective loss due to the absorption in metallic waveguide cladding on the order of $\text{Im}[k_z]/\text{Re}[k_z] \sim 10^{-3}$, in contrast to $\text{Im}[k_z]/\text{Re}[k_z] \sim 0.1$ in a hyperbolic waveguide.
- [25] S. Ramo, J. R. Whinnery, T. Van Duzer, “Fields and Waves in Communication Electronics,” John Wiley & Sons, Hoboken, 3rd edition (1994).
- [26] R. Wangberg, J. Elser, E. E. Narimanov, V. A. Podolskiy, “Non-magnetic nano-composites for optical and infrared negative refraction index media,” *J. Opt. Soc. Am. B* **23**(3), 498 (2006).
- [27] Note that the “ideal metal” boundary condition that sets the tangential electric field to zero, typically used at THz frequencies and below, does not at all actually assume an ideal/lossless metal, but only implies large *modulus* of the permittivity, regardless of whether its “lossless” ($|\text{Re}[\epsilon]| \gg \text{Im}[\epsilon]$) or extremely “lossy” ($|\text{Re}[\epsilon]| \ll \text{Im}[\epsilon]$). E.g. at GHz frequencies when the use of this approximation is nearly universal,[25] the dielectric permittivity of copper, the material often used for the microwave waveguides, is on the order of $10^8 i$.
- [28] Dyakonov, M. I., “New type of electromagnetic wave propagating at an interface,”. *Soviet Physics JETP* **67** (4), 714 (1988).
- [29] Walker, D. B., Glytsis, E. N. and Gaylord, T. K., “Surface mode at isotropic-uniaxial and isotropic-biaxial interfaces.” *J. Opt. Soc. Am.* **15**, 248 - 260 (1998).
- [30] O. Takayama *et al*, “Dyakonov Surface Waves: A Review,” *Electromagnetics* **28** (3), 126 - 145 (2008).
- [31] S. Hirotsu, T. Yanagi and S. Sawada, “Refractive Indices of NaN_2 and Anisotropic Polarizability of NO_2^- ,” *Journal of the Physical Society of Japan* **25** (3), 799 - 807 (1968).
- [32] F. D. M. Haldane, “Electromagnetic Surface Modes at Interfaces with Negative Refractive Index make a “Not-Quite-Perfect” Lens.” Preprint at <https://arxiv.org/abs/cond-mat/0206420> (2002).
- [33] L.D. Landau and E.M. Lifshitz, “Electrodynamics of Continuous Media,” Elsevier Butterworth-Heinemann; 2nd edition, Oxford (1984).